# Autonomous sweat extraction and analysis applied to cystic fibrosis and glucose monitoring using a fully integrated wearable platform

Sam Emaminejad[a,b,c,d,1,2], Wei Gao[b,c,d,1], Eric Wu[b], Zoe A. Davies[e], Hnin Yin Yin Nyein[b,c,d], Samyuktha Challa[a,f], Sean P. Ryan[e], Hossain M. Fahad[b,c,d], Kevin Chen[b,c,d], Ziba Shahpar[b,c,d], Salmonn Talebi[a,f], Carlos Milla[f,3], Ali Javey[b,c,d,3], and Ronald W. Davis[a,3]

[a]Stanford Genome Technology Center, Stanford School of Medicine, Palo Alto, CA 94304; [b]Department of Electrical Engineering and Computer Sciences, University of California, Berkeley, CA 94720; [c]Berkeley Sensor and Actuator Center, University of California, Berkeley, CA 94720; [d]Materials Sciences Division, Lawrence Berkeley National Laboratory, Berkeley, CA 94720; [e]The Stanford Cystic Fibrosis Center, Center for Excellence in Pulmonary Biology, Stanford School of Medicine, Palo Alto, CA 94305; and [f]Department of Electrical Engineering, Stanford University, Stanford, CA 94305

Contributed by Ronald W. Davis, February 14, 2017 (sent for review December 15, 2016; reviewed by Maneesh Jain and Andre Marziali)

**Perspiration-based wearable biosensors facilitate continuous monitoring of individuals' health states with real-time and molecular-level insight. The inherent inaccessibility of sweat in sedentary individuals in large volume (≥10 μL) for on-demand and in situ analysis has limited our ability to capitalize on this noninvasive and rich source of information. A wearable and miniaturized iontophoresis interface is an excellent solution to overcome this barrier. The iontophoresis process involves delivery of stimulating agonists to the sweat glands with the aid of an electrical current. The challenge remains in devising an iontophoresis interface that can extract sufficient amount of sweat for robust sensing, without electrode corrosion and burning/causing discomfort in subjects. Here, we overcame this challenge through realizing an electrochemically enhanced iontophoresis interface, integrated in a wearable sweat analysis platform. This interface can be programmed to induce sweat with various secretion profiles for real-time analysis, a capability which can be exploited to advance our knowledge of the sweat gland physiology and the secretion process. To demonstrate the clinical value of our platform, human subject studies were performed in the context of the cystic fibrosis diagnosis and preliminary investigation of the blood/sweat glucose correlation. With our platform, we detected the elevated sweat electrolyte content of cystic fibrosis patients compared with that of healthy control subjects. Furthermore, our results indicate that oral glucose consumption in the fasting state is followed by increased glucose levels in both sweat and blood. Our solution opens the possibility for a broad range of noninvasive diagnostic and general population health monitoring applications.**

wearable | biosensors | noninvasive | iontophoresis | personalized medicine

Wearable biosensors have received considerable attention owing to their great promise for a wide range of clinical and physiological applications (1–10). Despite significant progress made in printed and flexible biosensors in the field, a majority of wearable devices focus on monitoring of physical activity or selected electrophysiological parameters, providing only limited information regarding physiological changes of complex homeostatic responses (4–10). Wearable chemical sensors offer great opportunities for collecting physiological information at the molecular level (3, 9–19). Recently research advances have resulted in a variety of wearable sweat sensors that can be used for real-time analysis of sweat biomarkers including electrolytes, metabolites, and heavy metals (11–20). We recently demonstrated a fully integrated wearable sensing system for real-time monitoring of multiple analytes in human perspiration during physical exercise which allows accurate measurement of sweat analytes through signal processing and calibration (16).

The inherent inaccessibility of sweat in sedentary individuals in large volume (≥10 μL) for on-demand and in situ analysis remains to limit our ability to capitalize on this noninvasive and rich source of information for broad population monitoring. A wearable and miniaturized iontophoresis interface is an excellent solution to overcome this barrier. The iontophoresis process involves delivery of stimulating agonists to the sweat glands with the aid of an electrical current. The challenge remains in devising an iontophoresis interface that can extract and deliver sufficient amount of sweat to the sensor surface for robust sensing, without electrode corrosion and burning/causing discomfort in subjects.

Iontophoresis is currently a widely used method to stimulate local sweat secretion at a selected site (21). The conventional procedure involves stimulation, collection, and analysis all in separate steps, which not only requires extensive manual sample handling steps, but also fails to provide real-time insight into the secretion process. Despite the technological shortcomings, sweat analysis has shown great potential for a variety of clinical and physiological applications. For example, the sweat chloride level in iontophoresis-extracted sweat sample is currently considered the

## Significance

The inherent inaccessibility of sweat in sedentary individuals in large volume (≥10 μL) for on-demand and in situ analysis has limited our ability to capitalize on this noninvasive and rich source of information. Through devising an electrochemically enhanced, programmable, and miniaturized iontophoresis interface, integrated in a wearable sensing platform, we demonstrated a method for periodic sweat extraction and in situ analysis. The system can be programmed to induce sweat with various secretion profiles, which in combination with the in situ analysis capability allow us to gain real-time insight into the sweat-secretion and gland physiology. To demonstrate the clinical value of our platform, human subject studies were performed in the context of the cystic fibrosis diagnosis and preliminary investigation of the blood/sweat glucose correlation.

Author contributions: S.E., W.G., C.M., A.J., and R.W.D. designed research; S.E., W.G., E.W., Z.A.D., H.Y.Y.N., S.C., S.P.R., H.M.F., K.C., Z.S., S.T., C.M., A.J., and R.W.D. performed research; S.E., W.G., E.W., C.M., A.J., and R.W.D. contributed new reagents/analytic tools; S.E., W.G., E.W., C.M., A.J., and R.W.D. analyzed data; and S.E., W.G., E.W., C.M., A.J., and R.W.D. wrote the paper.

Reviewers: M.J., Cirina; and A.M., University of British Columbia.

The authors declare no conflict of interest.

Freely available online through the PNAS open access option.

[1]S.E. and W.G. contributed equally to this work.

[2]Present address: Department of Electrical Engineering, University of California, Los Angeles, CA 90095.

[3]To whom correspondence may be addressed. Email: cmilla@stanford.edu, ajavey@berkeley.edu, or krhong@stanford.edu.

This article contains supporting information online at www.pnas.org/lookup/suppl/doi:10.1073/pnas.1701740114/-/DCSupplemental.

gold standard for screening cystic fibrosis (CF), a genetic chronic disease that affects lungs and digestive system (21–23). A strong correlation between blood and sweat ethanol concentrations has been reported which could enable continuous blood-alcohol monitoring by sweat analysis (24, 25). In a recent work, real-time sweat ethanol monitoring using a wearable tattoo-based iontophoretic-biosensing system has been developed (20). Sweat extracted from iontophoresis has also been shown to contain glucose levels that can accurately reflect blood glucose (26).

Here, we devised an electrochemically enhanced iontophoresis interface which can extract sufficient sweat volume for robust analysis without causing discomfort in patients. This interface can be programmed to induce sweat periodically with various secretion profiles. Hence, it can be used to gain an unprecedented insight into the secretion process to advance the state of the science and our knowledge of the sweat gland physiology. Accordingly, we integrated this capability to demonstrate a fully integrated and autonomous platform that can stimulate sweat secretion and measure analytes of interest in the sweat collected (e.g., glucose, $Na^+$, and $Cl^-$) in situ and in real time (Fig. 1). The developed platform makes the physiologically rich sweat sample accessible on demand for general population health monitoring. As a result, it can be used for a wide range of applications in personalized medicine such as in-home continuous patient monitoring in response to potentially novel CF modulating drugs and enabling further clinical investigations including diabetes and prediabetes monitoring in a practical and noninvasive modality.

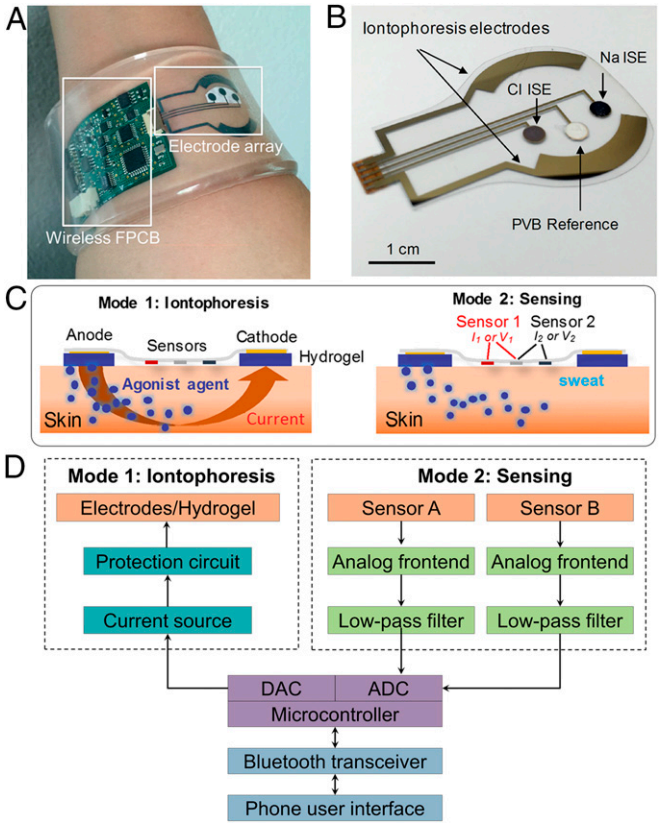


**Fig. 1.** (*A*) Image of the autonomous sweat extraction and sensing platform (a thin layer of agonist agent hydrogel will be placed underneath the iontophoresis electrodes). (*B*) Image of iontophoresis and sweat sensor electrodes for $Na^+$ and $Cl^-$ sensing. (*C*) Schematic illustrations of the iontophoresis and sensing modes. (*D*) System-level block diagram of the platform showing the iontophoresis and sensing circuits.

This system implements a wirelessly programmable iontophoresis capability to induce sweat with different excretion rate profiles and at periodic time intervals. Through integration of sensing electrodes on the same substrate as that of the iontophoresis electrodes, the induced sweat can be analyzed on-site immediately. The sensors are capable of quantifying sweat $Na^+$, $Cl^-$, and glucose, with high sensitivity in the physiologically relevant ranges of interest. As shown in Fig. 1, our platform consists of an electrode array, containing the sweat induction and sensing electrodes, integrated with a wireless flexible printed circuit board (FPCB). The independent functionality of the individual sensors and the iontophoresis process is preserved through electrically decoupling the switchable sweat sensing and sweat induction modes of operation (Fig. 1*C*).

The electrodes were patterned on a mechanically flexible polyethylene terephthalate (PET) substrate to form a stable sensor–skin contact (Fig. 1*B*). The sweat induction electrodes interface the skin with a thin layer of agonist agent hydrogel in between. To electrically connect the sweat induction electrodes and the hydrogels, thin stainless steel (corrosion-proof) contacts are used. The hydrogels are loaded with cholinergic sweat gland secretory stimulating compounds (e.g., pilocarpine). Depending on the devised compound formulation, different patterns of sweat secretion can be achieved. The sensing electrodes interface the skin through a water-absorbent thin rayon pad. To demonstrate the sweat analysis capability, we developed potentiometric sodium and chloride sensors, functionalized with ion-selective films (Fig. 1*B*), as well as an amperometric glucose sensor with the aid of glucose oxidase. The panel of target analytes was selected based on their informative role in terms of clinical diagnosis or providing understanding of an individual's physiological state. Specifically, sodium and chloride levels in sweat are diagnostic markers for CF, and glucose level in iontophoresis-induced sweat is reported to be potentially related to that in blood and thus applicable to diabetes screening and monitoring.

The FPCB module consolidates the required integrated circuit chips and peripheral electronics to implement iontophoresis, signal processing, control, and wireless transmission circuitries, thus delivering a fully integrated seamless and programmable system (Figs. S1–S3). Fig. 1*D* illustrates the system-level overview of the induction and sensing modes of operation. The sweat induction circuit consists of a programmable current source for iontophoresis current delivery and a protection circuit that sets an upper limit on the iontophoresis current as a safety mechanism to avoid overheating and burning the skin.

The sweat sensing circuit consists of two signal-conditioning paths in relation to the corresponding transduced signal, where each includes an analog front end to amplify the signal as well as a low-pass filter to minimize the high-frequency noise and electromagnetic interference (Fig. S2). The FPCB at its core uses a microcontroller that can be programmed to set the mode of operation through controlling a bank of switches to turn on/off the respective circuits and electrical paths. The microcontroller's digital-to-analog (DAC) port is used to drive the iontophoresis circuit and its analog-to-digital (ADC) port is used to convert the analog-processed signal into the digital domain. The microcontroller interfaces with an onboard wireless transceiver to communicate the incoming/outgoing data from/to a Bluetooth-enabled mobile handset with a custom-developed application. The mobile application has a user-friendly interface for programming the mode of operation as well as displaying and sharing the iontophoresis and sweat analysis data through email, short message service, and cloud servers (Fig. S4).

The iontophoresis circuit was implemented as a digitally programmable current source, ensuring that variation in the skin condition (such as thickness and conductivity) of individuals does not affect iontophoresis performance. Fig. 2*A* demonstrates the programmability and current source behavior of the circuit. The circuit delivers a current proportional to the output voltage of the microcontroller's DAC port, and this current is independent of load sizes ranging from 5 to 20 kΩ (the typical skin impedance in

our context is ~10 kΩ). The programmability of the current source circuit allows for inducing different iontophoresis current profiles, which in turn allows for sweat stimulation with controlled intensity and duration of sweat rate. Fig. 2 *B* and *C* illustrates our platform's capability to generate iontophoretic currents with a sawtooth wave profile (Fig. 2*B*) and a square wave profile (Fig. 2*C*).

The sensing electrodes of our platform can be modified differently according to the specific applications. Fig. 2 *D*–*F* illustrates examples of the modified electrochemical sensors for sweat chloride, sodium, and glucose analysis (the corresponding calibration curves are shown in Fig. S5). Ag/AgCl electrodes were chosen for chloride ion detection (23) whereas the measurement of sodium ions was achieved by using previously reported sodium ionophore X selectophore-based ion-selective electrodes (15). A polyvinyl butyral (PVB)-coated electrode containing saturated chloride ions was chosen as the reference electrode due to its stable potentials in different analyte solutions (16). The performance of $Na^+$ and $Cl^-$ sensor was characterized in different NaCl solutions with physiologically relevant concentrations. The potential differences between the ion-selective electrodes and the PVB-coated reference electrode were measured through a differential amplifier. Fig. 2 *D* and *E* shows the representative voltage responses of the $Na^+$ and $Cl^-$ sensors, measured in 10–160 mM NaCl solutions, respectively. Both ion-selective sensors show a near-Nernstian behavior with sensitivities of 63.2 and 55.1 mV per decade of concentration for $Na^+$ and $Cl^-$ sensors, respectively. Fig. S6 illustrates the long-term continuous measurement of a $Cl^-$ sensor over a 6-h period in 20, 40, and 80 mM NaCl solutions. The repeatability of the chloride sensors is demonstrated in Fig. S7. Three typical $Cl^-$ sensors show nearly identical absolute potentials in 10–80 mM NaCl solutions with a variation of <1% in sensitivity. Fig. 2*F* shows the chronoamperometric responses of a glucose sensor to glucose solutions with a typical sweat concentration range from 0 to 100 μM. The sensitivity of the glucose sensor is estimated as 2.1 nA/μM. Results of long-term stability studies of these electrochemical sensors indicate that the sensitivities of the biosensors are consistent over 2 wk with sensitivity variations of <5% (16).

By modulating the formulation of the compounds that are loaded into the iontophoresis hydrogel, we can achieve different patterns of sweat-secretion rate. We characterized the induced sweat rate profiles as stimulated by three different cholinergic agonist hydrogels (acetylcholine, methacholine, and pilocarpine) each at two different concentrations. For this characterization step, 2 mA of current over duration of 5 min was applied using a pair of ring-shaped electrodes (WR Medical Electronics Co., area: 4.3 $cm^2$), with the sweat-rate sensor (Q-sweat, WR Medical Electronics Co.) mounted on the positive electrode, sealing the stimulated area. As illustrated in Fig. 3*A*, for all of the formulations sweat secretion initiated in just a few minutes from the start of iontophoresis. In particular, acetylcholine hydrogel presented a high sweat-rate response [354 nL/min/$cm^2$ for 10% (wt/vol) acetylcholine] with a short-lived effect. This pattern is suitable for the case where periodic sweat sampling with short intervals is required. To demonstrate the periodic sweat stimulation capability, we used our integrated platform and custom-developed acetylcholine-based hydrogel to induce sweat repeatedly in the same area. To retrieve the induced sweat rate information, immediately after each stimulation step, the stimulated area was wiped dry and sealed with the commercial sweat-rate sensor (Q-sweat, WR Medical Electronics Co.). After each characterization step, the same hydrogels were reused for the subsequent stimulation. By modulating the duration of the applied iontophoresis as well as the concentration of the agonist agent, we were able to tune the active sweat-secretion window from a few minutes (Fig. 3*B*, acetylcholine 1%, iontophoresis current: 1 mA for 10 s) to tens of minutes (Fig. 3*C*, acetylcholine 10%, iontophoresis current: 1 mA for 5 min).

Furthermore, as shown in Fig. 3*A*, pilocarpine and methacholine-based hydrogels provide long duration of secretion beyond the 60-min characterization window, where about half of the secretion period was spent at about the peak rate. Specifically, methacholine at 10% concentration gave the optimal combination of a rapid onset of secretion with high secretory rate and sustained secretion at high rate that is also above the minimum recommended for sweat chloride analysis in CF (>100 nL/min/$cm^2$). Therefore, for subsequent on-body sweat extraction and sensing experiments we used this formulation for our hydrogels.

This integrated platform can be used both as a diagnostic and clinical investigation tool. To demonstrate its diagnostic capability, the platform was used in the context of CF. As a genetic disease, CF usually leads to an early death and is present in 1 out of every 3,000 newborn Caucasians. By current standards, sweat testing for CF diagnosis is performed by highly qualified certified laboratories in two steps: first, a sufficient amount of sweat is collected and then transferred for chloride content determination in a second step. Typically the test entails at least two technicians involved and takes a few hours to complete. A sweat chloride level of ≥60 mM is indicative of a high likelihood of CF, whereas in subjects with sweat chloride <30 mM the disease is unlikely (21). It is also known that the $Cl^-$-based sweat test and genetic analysis are not always sufficient for some CF patients with rare mutations whereas the ratio of the sweat sodium and chloride levels can aid the CF diagnosis (27). Our device can potentially serve as a reliable tool for early screening of cystic fibrosis through on-demand sweat stimulation and simultaneous sodium and chloride sensing in sweat. The

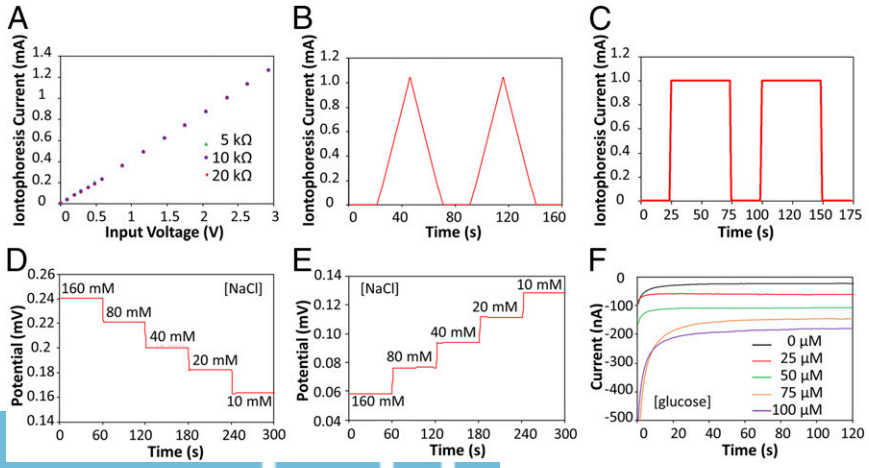


**Fig. 2.** Experimental characterizations of the iontophoresis and sensing system. (*A*) Controlled iontophoresis current output for various resistive loads. (*B* and *C*) Programmed iontophoresis current to generate (*B*) sawtooth and (*C*) square wave patterns. (*D* and *E*) The open-circuit potential responses of the sodium (*D*) and chloride (*E*) sensors in NaCl solutions. (*F*) The chronoamperometric responses of a glucose sensor to glucose solutions. Data recording was paused for 30 s for each solution change.

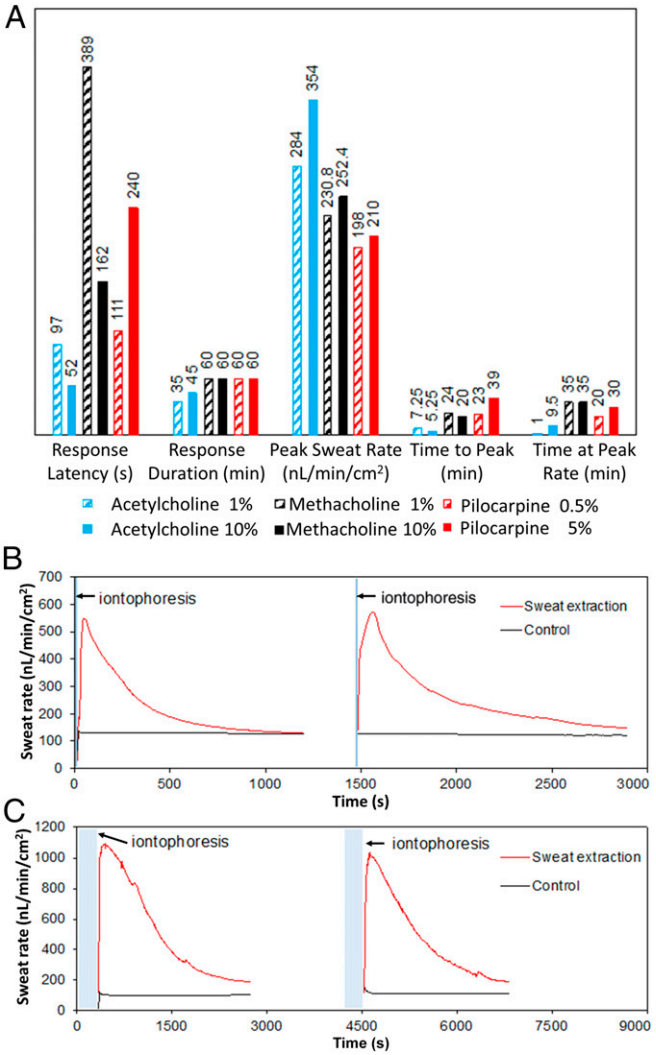


**Fig. 3.** (*A*) Induced sweat-secretion rate characteristics in response to three different custom-developed cholinergic agonist hydrogels with two different concentrations: acetylcholine (blue), methacholine (black), and pilocarpine (red). Bars represent values for response latency (time in seconds to onset of secretion from start of iontophoresis), response duration (total time in minutes of secretion above baseline, measurements stopped at 60 min), peak secretory rate in response to stimulation, time to reach peak secretory rate, and time spent secreting at the peak rate. (*B*) Sweat-rate profile pertaining to periodic sweat induction using acetylcholine 1%-based hydrogel with iontophoresis current of 1 mA for 10 s. (*C*) Sweat-rate profile pertaining to periodic sweat induction using acetylcholine 10%-based hydrogel with iontophoresis current of 1 mA for 5 min (bottom panel). The control curves in *B* and *C* represent the sweat-rate profile in the contralateral arm without iontophoresis.

repeated sweat extraction and sensing is also very useful for monitoring the severity and recovery of CF patients. In this case, the wearable system is packaged in a smart wristband and worn by the subjects. A 1-mA current is applied onto the skin for 10 min, which effectively delivers cholinergic agonists to the dermal space to reach the sweat glands and induce sweating. When sweating begins, the sensors measure potential differences between the reference and the working electrodes. The response stabilizes at ~20 min after iontophoresis, indicating that sufficient sweat has been generated. Fig. 4 *A* and *B* illustrates the real-time on-body measurement (20~25 min) sweat electrolyte levels for a representative healthy subject and a CF patient, respectively (full data illustrated in Fig. S8). It can be clearly observed that both $Na^+$ and $Cl^-$ levels for the healthy subjects fall below 20 mM while the patient has higher sweat $Na^+$ and $Cl^-$ levels (>60 mM). In situ sweat analysis using our wearable system was performed on six healthy volunteers and three CF patients. As displayed in Fig. 4*C*, the average sodium and chloride levels (based on the sensor readings at 25 min) for healthy subjects are 26.7 and 21.2 mM, respectively, while the average sodium and chloride levels (based on the sensor readings at 25 min) for CF patient subjects are 82.3 and 95.7 mM, respectively. It should be noted that, in agreement with a previous report (27), sweat sodium levels are lower than sweat chloride levels for CF patient subjects in contrast to healthy subjects where sweat sodium levels are higher, indicating another method to consolidate the screening assessment of CF.

Furthermore, we can use our platform as an investigation tool to enable a wide range of clinical and physiological applications. As an additional potential application, with our platform we conducted preliminary studies toward understanding the metabolic correlation of glucose content in iontophoresis induced sweat vs. blood. Although there is literature reporting that sweat glucose level is related with blood glucose level (26), their metabolic correlation has not been well studied. To evaluate the utility of our wearable platform for noninvasive glucose monitoring, real-time sweat stimulation and glucose-sensing measurements were conducted on a group of subjects engaged in both fasting and postglucose intake trials.

Fig. 5 illustrates that the sweat and blood glucose levels of seven healthy subjects before and after glucose intake (30 g oral glucose) follow a similar pattern. Here, the blood glucose analysis is performed using a commercially available glucometer (GE100, Bionime Corp.). The off-body measurement results from the collected sweat sample induced by our wearable device indicate that oral glucose consumption in fasting subjects usually results in increase of glucose level in both sweat and blood (from six out of seven subjects). To get more accurate measurements of sweat glucose level and a further understanding of the correlation between sweat and blood glucose levels, future work will involve the integration of the temperature, pH, and sweat-rate sensors to calibrate the glucose measurements in sweat.

In conclusion, we have demonstrated a fully integrated and autonomous platform that enables continuous and noninvasive monitoring of individuals. This platform extracts sweat (at a high secretion rate) on demand or periodically and performs sweat analysis in situ. Through optimization of sweat-stimulating drug concentration in the custom-developed hydrogels and careful design of the iontophoresis electrodes, we were able to consistently achieve secretory rates in excess of 100 nL/min/cm$^2$ and extract sufficient amounts of sweat for reliable analysis without causing skin damage or discomfort in the subjects. Additionally, incorporation of simultaneous in situ analysis functionality inherently allowed for significant reduction of the sweat sample degradation, evaporation, or contamination. To illustrate the value of our solution as a diagnostic tool, we used the platform to detect the elevated sweat sodium and chloride ions content in the CF patients. Furthermore, to demonstrate the utility of the platform as a clinical and physiological investigation tool, we applied our solution to conduct a preliminary study toward understanding the metabolic correlation of glucose content in sweat vs. blood. To precisely establish the correlation between the sweat and blood glucose, in the future sweat-rate monitoring functionality can be integrated to allow for normalization of the analyte content with respect to the sweat-rate information of the individual. Furthermore, future efforts will be focused on integration of a wider panel of biomarker, and peripheral electrochemical and physical (e.g., pH and temperature) sensors to deliver a versatile wearable platform for large-scale clinical and physiological investigations. We envision that through enabling such large-scale studies, our platform would help to establish the relationship between the sweat profile and the physiological state of the individuals, hence paving the way for adoption of sweat-based sensing as a noninvasive and seamless method of diagnosis and screening for general population.

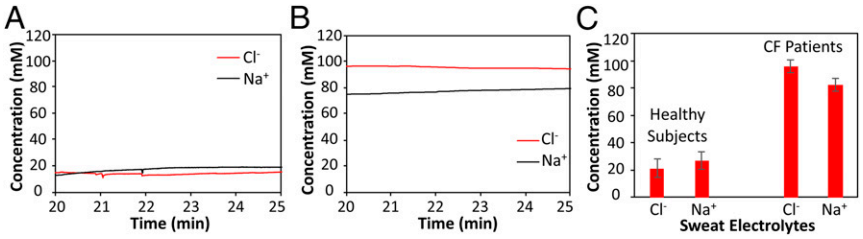


**Fig. 4.** Wearable sweat extraction and sensing system for CF diagnosis. (*A*) Real-time on-body measurement of sweat sodium ion and chloride ion levels of a healthy subject after iontophoresis-based sweat stimulation. (*B*) Real-time measurement of sweat sodium and chloride levels of a CF patient. (*C*) Comparison of sweat electrolyte levels between six healthy subjects and three CF patients.

## Materials and Methods

**Materials.** Selectophore-grade sodium ionophore X, bis(2-ethylehexyl) sebacate (DOS), sodium tetrakis[3,5-bis(trifluoromethyl)phenyl] borate (Na-TFPB), high-molecular-weight polyvinyl chloride (PVC), tetrahydrofuran, sodium tetraphenylborate (NaTPB), cyclohexanone, polyvinyl butyral resin BUTVAR B-98 (PVB), sodium chloride (NaCl), 3,4-ethylenedioxythiophene (EDOT), poly(sodium 4-styrenesulfonate) (NaPSS), glucose oxidase (from *Aspergillus niger*), chitosan, single-walled carbon nanotubes, iron (III) chloride, potassium ferricyanide (III), were purchased from Sigma-Aldrich. Moisture-resistant 100-μm-thick PET was from McMaster-Carr. All reagents were used as received.

**Fabrication of Electrodes Array.** The fabrication process takes similar steps as in a previous paper (16). In brief, PET is cleaned with isopropyl alcohol and $O_2$ plasma etching. An electrode array of 3.2 mm diameter is patterned via photolithography and is thermally evaporated with 30/100 nm of Cr/Au, followed by lift-off in acetone. The electrode array is additionally coated with 500-nm parylene C insulation layer in an SCS Labcoter 2 Parylene Deposition System, and the 3-mm-diameter sensing electrode area is defined via photolithography. The fabricated array is further etched with $O_2$ plasma to remove the parylene layer at the defined sensing area. Finally, 200 nm Ag is deposited via thermal evaporation and lift-off in acetone.

**Preparation of $Na^+$- and $Cl^-$-Selective Sensors.** The $Cl^-$-selective Ag/AgCl electrode was prepared obtained by injecting 10 μl 0.1-M $FeCl_3$ solution on top of evaporated Ag electrode using a micropipette for 1 min. The $Na^+$-selective membrane mixture consisted of Na ionophore X (1% weight by weight, wt/wt), Na-TFPB (0.55% wt/wt), PVC (33% wt/wt), and DOS (65.45% wt/wt). Next, 100 mg of the membrane mixture was dissolved in 660 μl of tetrahydrofuran. The ion-selective solutions were sealed and stored at 4 °C. The solution for the PVB reference electrode was prepared by dissolving 79.1 mg PVB and 50 mg of NaCl into 1 ml methanol.

Poly(3,4-ethylenedioxythiophene) PEDOT:PSS was chosen as the ion–electron transducer to minimize the potential drift of the ion-selective electrodes (ISEs) and deposited onto the working electrodes by galvanostatic electrochemical polymerization with an external Ag/AgCl reference electrode from a solution containing 0.01M EDOT and 0.1 M NaPSS. A constant current of 14 μA (2 mA $cm^{-2}$) was applied to produce polymerization charges of 10 mC onto each electrode.

Ion-selective membranes were then prepared by drop-casting 10 μl of the $Na^+$-selective membrane mixture onto the corresponding electrodes. The common reference electrode for the $Na^+$ and $Cl^-$ ISEs was modified by casting 10 μl of reference solution onto the Ag/AgCl electrode. The modified electrodes were left to dry overnight. However, to obtain the best performance, the ion-selective sensors were covered with a solution containing 50 mM NaCl through microinjection for 1 h before measurements. This conditioning process was important to minimize the potential drift.

**Preparation of Glucose Sensors.** First, 1% chitosan solution was prepared by dissolving chitosan in 2% acetic acid and magnetic stirring for about 1 h; next, the chitosan solution was mixed with single-walled carbon nanotubes (2 mg $ml^{-1}$) by ultrasonic agitation over 30 min to prepare a viscous solution of chitosan and carbon nanotubes. To prepare the glucose sensors, the chitosan/carbon nanotube solution was mixed thoroughly with glucose oxidase solution (10 mg $ml^{-1}$ in PBS of pH 7.2) in the ratio 2:1 (volume/volume). A Prussian blue mediator layer was deposited onto the Au electrodes by cyclic voltammetry from 0 to 0.5 V (versus Ag/AgCl) for one cycle at a scan rate of 20 mV $s^{-1}$ in a fresh solution containing 2.5 mM $FeCl_3$, 100 mM KCl, 2.5 mM $K_3Fe(CN)_6$, and 100 mM HCl. The glucose sensor was obtained by drop-casting 3 μl of the glucose oxidase/chitosan/carbon nanotube solution onto the Prussian blue/Au electrode. The sensor arrays were allowed to dry overnight at 4 °C with no light. The solutions were stored at 4 °C when not in use.

**Preparation of Agonist Agent Hydrogels.** Hydrogels with cholinergic agonists at different concentrations were prepared based on previously reported methods (28). In brief, a 3% agarose gel was prepared in a glass beaker by melting the agarose in water for 1 min in a microwave. The liquefied hot gel was allowed to cool down to 47 °C, a magnetic stirrer was dropped into the beaker, and this was placed on a hot plate stirrer set at 47 °C. Then, the appropriate amount of the agonist solution was added to make the desired final concentration and allowed to mix well by stirring for 1 min. The melted gel was then poured into cylindrical molds and allowed to solidify for 1 h at 4 °C. Next, the hardened gel was sliced in 1-mm disks which were in turn cut with the aid of metal dies to the shape of the iontophoresis electrodes before application to the subject's skin.

**Overall System Design.** The overall system was based around the Atmel ATmega328P 8-bit microcontroller with accompanying analog circuitry for both sensor reading and iontophoresis current delivery. The microcontroller's onboard 10-bit ADC was used to both read sensor data and to monitor iontophoresis current. A Bluetooth transceiver was connected to the microcontroller to interface the system to a cell phone. Using the cell phone, the

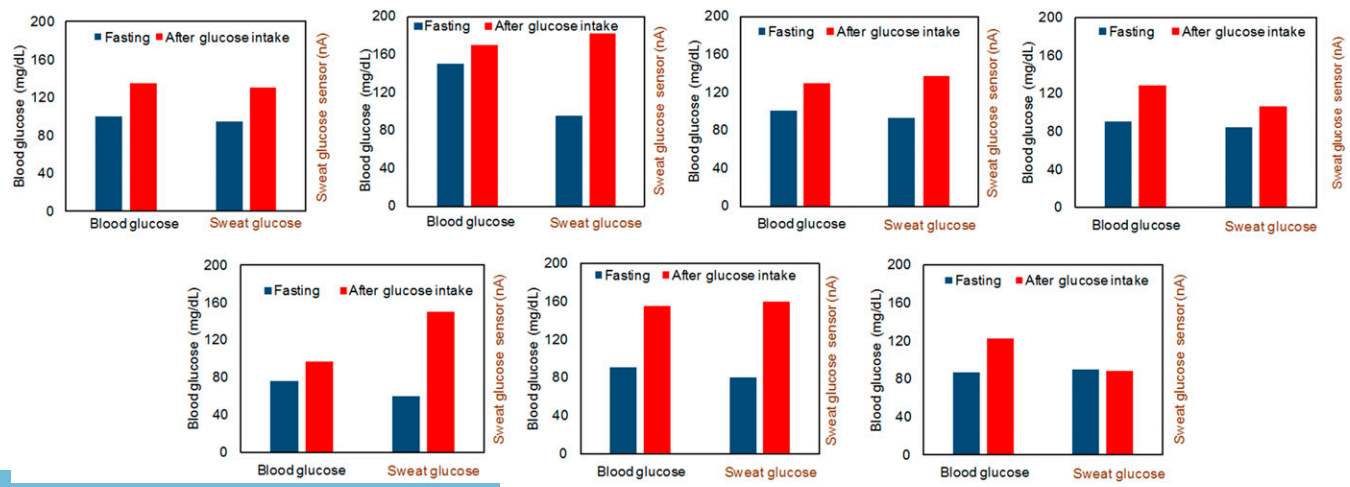


**Fig. 5.** Comparison of the blood and sweat glucose levels of seven subjects during 12-h fasting and 1 h after glucose intake (30 g glucose).

system could be commanded to output varying levels of iontophoresis current or to transmit sensor readings in real time.

**Signal-Conditioning Circuit Design and Processing.** Low-leakage analog switches were used to interface between the sensors and the beginning of the analog signal-conditioning circuits. The state of these switches was digitally controlled by the microcontroller, and the switches were set to high impedance (open circuit) during iontophoresis to protect the signal-conditioning circuitry and to minimize the possibility of burning the test subject.

The signal-conditioning circuitry was implemented in relation to the corresponding sensing mode. For the amperometric glucose sensors, the sensor output is in the form of an electrical current, necessitating the use of a transimpedance amplifier (TIA) first stage to amplify the signal and to convert it from a current to a voltage. A 1-MΩ resistor was placed in feedback for the TIA to set the current-to-voltage gain to $-10^6$, to allow us to measure current with nanoampere precision. Because the sensor outputs positive current from the Ag/AgCl reference electrode toward the working electrode, and because the TIA has a negative gain, the Ag/AgCl reference electrode was biased to +2.5 V to keep the signal within 0–5-V range of the microcontroller's ADC. For the potentiometric $Na^+$ and $Cl^-$ sensors, the sensor output is in the form of a differential voltage. The first stage for the potentiometric sensing channels consisted of Analog Devices AD8422 instrumentation amplifiers with gain set to 5, providing high impedance inputs for the sensors with maximal common-mode noise rejection. By setting the first stage gain to 5, we were able to achieve millivolt-level resolution over the physiologically relevant range of $Na^+$ and $Cl^-$ concentrations. The PVB reference electrode for the potentiometric sensors was allowed to float, with a 10-kΩ resistor to +2.5 V to provide a path for the input bias current for the amplifiers. The reference terminals of the instrumentation amplifiers were tied to +2.5 V to allow for maximal output swing in single-supply operation.

All of the analog signal-conditioning paths were terminated with a four-pole unity gain low-pass filter, with −3dB frequency set to 1 Hz to minimize noise and interference in the measurements. The filter outputs were connected to the 10-bit ADC on the microcontroller. ADC readings were oversampled 1,000× in software on the microcontroller to further improve resolution and accuracy. These readings were then relayed over Bluetooth to cell phone.

Schematics for the analog signal-conditioning circuitry are shown in Fig. S2.

**Iontophoresis Current Delivery and Protection Circuit Design.** To deliver a wirelessly controllable iontophoresis current through loads of varying resistance, we designed a current DAC and protection circuitry to interface with the microcontroller. A second-order low-pass filter followed by voltage buffer was connected to a microcontroller output pin to convert the ATmega328P's pulse-width-modulated output to a dc voltage. This voltage was then used to control a voltage-controlled current source, based on an AD8276 difference amplifier with an external bipolar junction transistor output stage. This architecture enabled us to use Bluetooth commands to control delivery of iontophoresis currents to the test subject, and allowed us to program iontophoresis currents with arbitrary ramp-up/ramp-down profiles.

An ammeter based on the INA282 high-side current shunt monitor was placed in series with the current DAC, and the output was connected to one of the microcontroller's ADC channels to provide real-time monitoring of current delivery, and to enable the microcontroller to shut off current output if excessive current was being drawn. A junction field-effect transistor and 250-Ω series resistor were placed in series with the current path as a safety measure to ensure a maximum short-circuit current of 2 mA. Lastly, analog switches were placed at both positive and negative iontophoresis terminals to fully shut off current when necessary.

A schematic showing the current delivery circuitry is given in Fig. S3.

**Power Distribution.** The system was powered by a single rechargeable lithium-ion polymer battery with a nominal supply voltage of 3.7 V. A single +5-V boost regulator was used to generate the supply voltages for the microcontroller and for the analog signal-conditioning blocks. A +2.5-V virtual ground was used to bias the sensors at midsupply and to enable efficient, single-supply operation of the analog blocks. A +36-V boost regulator was used to generate the supply voltage for the current DAC, to ensure that the system could deliver appropriate amounts of iontophoresis current through a wide range of physiologically relevant resistive loads. Lastly, a 3.3-V low-dropout regulator was used to provide power for the Bluetooth module.

**The Setup of Wearable System for On-Body Testing.** A water-absorbent thin rayon pad was placed between the skin and the sensor array during on-body experiments to absorb and maintain sweat for stable and reliable sensor readings, and to prevent direct mechanical contact between the sensors and skin. The on-body measurement results were also consistent with ex situ tests using freshly collected sweat samples. The on-body evaluation of the wearable platform was performed in compliance with the protocols that were approved by the Institutional Review Board at University of California, Berkeley (2015-05-7578) and the Institutional Review Board at Stanford University (no. 31310). All subjects gave written, informed consent before participation in the study.

**ACKNOWLEDGMENTS.** The work at Stanford University was supported by the National Institutes of Health Grant P01 HG000205; the work at University of California, Berkeley was supported by National Science Foundation Nanomanufacturing Systems for Mobile Computing and Energy Technologies Center. The sensor fabrication was performed in the Electronic Materials Laboratory (funded by the Director, Office of Science, Office of Basic Energy Sciences, Material Sciences and Engineering Division of the US Department of Energy under Contract DE-AC02-05CH11231) and Stanford Nanofabrication Facility. K.C. acknowledges support from the Robert N. Noyce Fellowship in Microelectronics.

1. Kim DH, et al. (2011) Epidermal electronics. *Science* 333(6044):838–843.
2. Hammock ML, Chortos A, Tee BC, Tok JB, Bao Z (2013) 25th anniversary article: The evolution of electronic skin (e-skin): A brief history, design considerations, and recent progress. *Adv Mater* 25(42):5997–6038.
3. Bandodkar AJ, Jeerapan I, Wang J (2016) Wearable chemical sensors: Present challenges and future prospects. *ACS Sens.* 1:464–482.
4. Wang C, et al. (2013) User-interactive electronic skin for instantaneous pressure visualization. *Nat Mater* 12(10):899–904.
5. Xu S, et al. (2014) Soft microfluidic assemblies of sensors, circuits, and radios for the skin. *Science* 344(6179):70–74.
6. Kaltenbrunner M, et al. (2013) An ultra-lightweight design for imperceptible plastic electronics. *Nature* 499(7459):458–463.
7. Tee BCK, et al. (2015) A skin-inspired organic digital mechanoreceptor. *Science* 350(6258):313–316.
8. Takei K, Honda W, Harada S, Arie T, Akita S (2015) Toward flexible and wearable human-interactive health-monitoring devices. *Adv Healthc Mater* 4(4):487–500.
9. Chen K, et al. (2016) Printed carbon nanotube electronics and sensor systems. *Adv Mater* 28(22):4397–4414.
10. Imani S, et al. (2016) A wearable chemical-electrophysiological hybrid biosensing system for real-time health and fitness monitoring. *Nat Commun* 7:11650.
11. Bandodkar AJ, et al. (2014) Epidermal tattoo potentiometric sodium sensors with wireless signal transduction for continuous non-invasive sweat monitoring. *Biosens Bioelectron* 54:603–609.
12. Huang X, et al. (2014) Stretchable, wireless sensors and functional substrates for epidermal characterization of sweat. *Small* 10(15):3083–3090.
13. Rose DP, et al. (2015) Adhesive RFID sensor patch for monitoring of sweat electrolytes. *IEEE Trans Biomed Eng* 62(6):1457–1465.
14. Bandodkar AJ, et al. (2015) Tattoo-based noninvasive glucose monitoring: a proof-of-concept study. *Anal Chem* 87(1):394–398.
15. Schazmann B, et al. (2010) A wearable electrochemical sensor for the real-time measurement of sweat sodium concentration. *Anal Methods* 2:342–348.
16. Gao W, et al. (2016) Fully integrated wearable sensor arrays for multiplexed in situ perspiration analysis. *Nature* 529(7587):509–514.
17. Lee H, et al. (2016) A graphene-based electrochemical device with thermoresponsive microneedles for diabetes monitoring and therapy. *Nat Nanotechnol* 11(6):566–572.
18. Gao W, et al. (2016) Wearable microsensor array for multiplexed heavy metal monitoring of body fluids. *ACS Sens.* 1:866–874.
19. Nyein HY, et al. (2016) A Wearable electrochemical platform for non-invasive simultaneous monitoring of $Ca^{2+}$ and pH. *ACS Nano* 10(7):7216–7224.
20. Kim J, et al. (2016) Noninvasive alcohol monitoring using a wearable tattoo-based iontophoretic-biosensing system. *ACS Sens*, 10.1021/acssensors.6b00356.
21. Farrell PM, et al. (2017) Diagnosis of cystic fibrosis: Consensus guidelines from the Cystic Fibrosis Foundation. *J Pediatr* 181S:S4–S15, 15.e1.
22. Gibson LE, Cooke RE (1959) A test for concentration of electrolytes in sweat in cystic fibrosis of the pancreas utilizing pilocarpine by iontophoresis. *Pediatrics* 23(3):545–549.
23. Gonzalo-Ruiz J, et al. (2009) Early determination of cystic fibrosis by electrochemical chloride quantification in sweat. *Biosens Bioelectron* 24(6):1788–1791.
24. Buono MJ (1999) Sweat ethanol concentrations are highly correlated with co-existing blood values in humans. *Exp Physiol* 84(2):401–404.
25. Gamella M, et al. (2014) A novel non-invasive electrochemical biosensing device for in situ determination of the alcohol content in blood by monitoring ethanol in sweat. *Anal Chim Acta* 806:1–7.
26. Moyer J, Wilson D, Finkelshtein I, Wong B, Potts R (2012) Correlation between sweat glucose and blood glucose in subjects with diabetes. *Diabetes Technol Ther* 14(5):398–402.
27. Augarten A, et al. (1995) The significance of sweat Cl/Na ratio in patients with borderline sweat test. *Pediatr Pulmonol* 20(6):369–371.
28. Sletten DM, Kimpinski K, Weigand SD, Low PA (2009) A novel gel based vehicle for the delivery of acetylcholine in quantitative sudomotor axon reflex testing. *Auton Neurosci* 150(1-2):127–130.